Journal of Power Sources 194 (2009) 20–24

Contents lists available at ScienceDirect

Journal of Power Sources

journal homepage: www.elsevier.com/locate/jpowsour

Short communication

Interaction of yttria stabilized zirconia electrolyte with Fe_2O_3 and Cr_2O_3

Sebastian Molin[a,*], Maria Gazda[b], Piotr Jasinski[a]

[a] Faculty of Electronics, Telecommunications and Informatics, Gdansk University of Technology, ul. Narutowicza 11/12, 80-952 Gdansk, Poland
[b] Faculty of Applied Physics and Mathematics, Gdansk University of Technology, ul. Narutowicza 11/12, 80-952 Gdansk, Poland

ARTICLE INFO

Article history:
Received 15 October 2008
Received in revised form 27 December 2008
Accepted 14 January 2009
Available online 21 January 2009

Keywords:
Fuel cell
YSZ electrolyte
Impedance spectroscopy
Iron oxide
Chromium oxide

ABSTRACT

Yttria stabilized zirconia electrolytes were sintered with addition of iron oxide or chromium oxide. The phase composition of the composites, sintering properties and DC and AC electrical properties are evaluated and compared with available data. Results show, that after sintering there is only single-phase material found in the XRD patterns. Iron can be considered as a sintering promoter while chromium decreases the apparently sintering process. Addition of either oxide decreases total electrical conductivity in comparison to pure samples. Based on impedance spectra it can be concluded that chromium mainly influences electrical conductivity of grain boundary, while iron influences electrical conductivity of both grain and grain boundary, with a solubility limit at grain boundaries estimated at about 2 mol% Fe.

1. Introduction

The yttria stabilized zirconia (YSZ) is a material of choice for solid oxide fuel cells electrolyte [1]. It has relatively high ionic conductivity at elevated temperatures, low thermal expansion coefficient, very good stability in both reducing and oxidizing gases and many more advantageous properties. In a fuel cell, the electrolyte material is in contact with anode and cathode. Therefore, studies of the possible interaction of electrolytes and other materials are very important. So far much work was done on the interaction of YSZ electrolyte with cathode materials [2]. Also interactions of YSZ with Mn_2O_3 [3] and TiO_2 [4] were studied. One of the new trends in the development of the next generation solid oxide fuel cells is the use of stainless steel as an interconnector or even as a supporting material in porous form [5,6]. Stainless steels that are regarded for SOFC applications include mainly ferritic steels based on iron (~75 wt%) and chromium (~20 wt%) with some minor additions – Mn, Co, Ni, Si, Mo. During high temperature oxidation processes the metal oxides are formed on the surface of steel. Understanding the interaction of electrolyte material with these oxides is becoming a basic need.

So far only a few scientific reports were related to the possible reaction of Fe or Cr with YSZ [7–15]. Some of them omit investigation of the electrical properties of structures resulted from this interaction. Davison et al. [7] performed X-ray powder diffraction analysis and magnetic measurements that indicated that α-Fe_2O_3 and ZrO_2 form a solid solution up to 25 at% Fe/Zr. Berry et al. [8] showed that zirconia cubic structure can be stabilized by the incorporation of Fe^{3+} into ZrO_2 at moderate temperatures (ca. 500 °C). This effect was associated with the presence of interstitial Fe^{3+} ions and oxygen vacancies. Rise of the processing temperature to approximately 1000 °C induces the transition back to the monoclinic ZrO_2. Simultaneously, iron partially segregates in the form of iron (III) oxide with possible zirconium additions. Gokon et al. [9] were considering iron containing YSZ for a two-step thermochemical water splitting applications. The authors considered a composite of YSZ with the addition of 18 wt% Fe_3O_4. After high temperature reduction of Fe_3O_4 to FeO iron was dissolved into YSZ lattice. Nakajima et al. [10] evaluated the effect of Fe doping on crystalline and optical properties of YSZ. The authors revealed that Fe ions are present on the surface and in the grain boundaries of Fe-doped YSZ as either nanocrystalline or amorphous oxides, which may not be detected by XRD. Gao et al. [11] evaluated the effect of iron doping on the properties of YSZ electrolyte for SOFCs. They prepared pure and doped YSZ (with 2 mol% and 4 mol% of Fe) sintered at 1200 °C and 1400 °C. Authors found that Fe ions can be dissolved in YSZ and as a result a decrease of the lattice parameter occurs. They observed also that Fe improved sinterability. For example, the samples containing iron sintered at 1200 °C were more dense than the undoped ones. On the other hand, the samples sintered at 1400 °C showed the decrease of the total electrical conductivity with the increase of the Fe content. In contrast to lower conductivity, the cells prepared from the Fe-doped YSZ showed better electrochemical performance, which was accounted for improved electrolyte–electrode interface. This effect was also previously reported by McDonald et al. [12].

* Corresponding author. Tel.: +48 58 347 25 09; fax: +48 58 347 17 57.
E-mail address: molin@biomed.eti.pg.gda.pl (S. Molin).

0378-7753/$ – see front matter © 2009 Elsevier B.V. All rights reserved.
doi:10.1016/j.jpowsour.2009.01.031

Impedance spectroscopy studies of iron- and titanium-doped YSZ were performed by Matsui [13,14]. Author concluded that iron dissolves into YSZ lattice and improves sinterability. By impedance measurements, the effect of iron on the electrical conductivity was assessed. Both grain and grain boundary contributions to conductivity were analyzed. In comparison to undoped samples, the iron doping lowers the grain conductivity. However, the iron level has no effect on the resistivity of grains. In case of the grain boundary resistivity, it is lowered when iron content is increased so in this case the iron improves electrical conductivity of grain boundary.

The results obtained in the works mentioned above do not answer all the questions concerning Fe and YSZ interaction. Moreover, some reported results are not consistent with each other. It can be explained by fact, that the samples studied were prepared by several different methods.

The iron-doped YSZ powder studied in this work was prepared by similar method as Gao et al. [11]. The high temperature sintering was performed on the samples prepared by mixing previously obtained powders of YSZ with the Fe_2O_3 and Cr_2O_3. This procedure corresponds to the situation that may occur in the stainless steel supported SOFCs. In this case the YSZ powders are sintered directly on stainless steel substrate, on which metal oxides might form and make contact with electrolyte. These differences in powder preparation procedures must be taken into account when comparing data. In general it might be stated that there is a lack of experimental data for explanation of the possible effects of Fe and Cr incorporation into YSZ electrolyte.

2. Experimental

Metal oxides were prepared by thermal decomposition of appropriate metal nitrates (Sigma–Aldrich, USA) at 800 °C for 2 h. Their purity and structure was confirmed by XRD measurements. The samples of YSZ with metal oxide addition were prepared by mixing commercial 8 mol% Y_2O_3-doped ZrO_2 powder (8-HSY, DKKK, Japan) with prepared Fe_2O_3 and Cr_2O_3 powders. Batches with 0 mol%, 1 mol%, 2 mol%, 4 mol% and 6 mol% of metal oxides were prepared. For example, sample denoted as 94YSZ6Fe has the following composition: 94 mol% of YSZ and 6 mol% of $FeO_{1.5}$. Powders after initial weighting were thoroughly milled in an agate mortar and pressed uniaxially in a steel die under a pressure of 100 MPa applied for 120 s. Each sample after compaction had a mass of approximately 0.8 g and diameter of 16 mm. The samples were sintered at 1200 °C and 1400 °C for 4 h. Ramp rates were 120° h^{-1} for heating and 140° h^{-1} for cooling.

Porosities of the samples were measured using Archimedes method with kerosene as a working liquid. X-ray diffractometry was performed by Philips X'Pert system with Cu Kα radiation. All scans were collected at room temperature in a standard 2θ setup. Electrical measurements were performed in both DC and AC modes. DC van der Pauw method was applied at high temperatures, namely higher than 500 °C, where conductivity contributions of grains and grain boundaries could not be resolved. The measurements were carried out in the temperature range from 800 °C to 500 °C with 50 °C steps. Silver paint (4922N, DuPont, USA) was used to attach four platinum wires to circular samples. At temperatures lower than 500 °C impedance spectroscopy measurements were performed. The samples were painted with the platinum paste (ESL 5542, USA) to form circular electrodes with diameter of approximately 10 mm and sintered at 910 °C for 10 min. This structure was then placed in a 2-wire spring loaded measurement cell. A Solartron 1260 Frequency Response Analyzer coupled with Solartron 1294 Impedance Interface was used. An excitation voltage of 100 mV was applied for all measurements in the frequency range of 1 MHz–1 Hz. For data analysis a ZView program (Scribner Associates, USA) was used. All electrical measurements were carried out in a tube furnace in air.

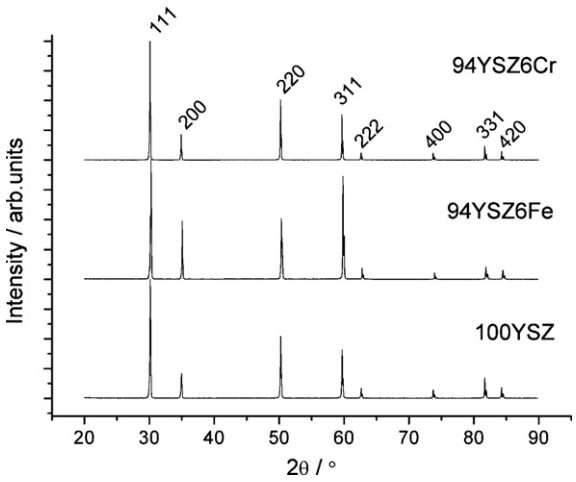

Fig. 1. XRD patterns of pure YSZ and Fe- and Cr-doped samples. All the reflexes are associated with the cubic fluorite unit cell (ICDD card number 30-1468).

3. Results and discussion

The results of the XRD measurements of samples with the highest, 6 mol% oxide composition levels are shown in Fig. 1. In each case all of the peaks can be attributed to the simple fluorite type cubic cell of YSZ (ICDD card number 30-1468). The reflections characteristic of oxide phases are not seen. In the case of other powders, with lower metal content, similar results are achieved. All of them were single-phased with no trace of metal oxides. The absence of reflections of oxides can be explained by a total dissolution of metal cations into YSZ lattice without change of crystal structure. The solubility limit for the materials prepared in this work is most probably on the level of at least 6 mol% of iron and chromium. In the case of iron the solubility limit of 8.06 mol% of Fe was reported by Wilhelm and Howarth [15] and confirmed by Gao et al. [11] and Matsui [13]. Information about Cr solubility in YSZ is not known. However, it should also be taken into consideration that the absence of the XRD reflections of oxide phases can be caused by the fact that oxides are present in the grain boundaries of Fe-doped YSZ as either nanocrystalline or amorphous, what was suggested by Nakajima et al. [10]. In order to further investigate whether the dopants dissolve into the YSZ the unit cell parameters of the studied materials were determined. The analysis was performed by the Rietveld refinement method. In case of the iron-doped YSZ the cubic unit cell parameter changed from 5.1351(1) Å to 5.1311(1) Å, whereas in the chromium-doped samples from 5.1386(2) Å to 5.1325(1) Å for 1 mol% and 6 mol% content of the dopant, respectively. Therefore, the unit cell parameters tend to decrease with the increase of the metal dopant content. This is consistent with work reported by Gao et al. [11] and Matsui [13]. To complete the analysis further investigations are necessary.

After the sintering step, porosity of all samples was measured. The results are presented in Fig. 2. The porosity of pure YSZ sintered at 1400 °C is approximately 3.6%. The lowest porosity for this sintering temperature is obtained for sample 99YSZ1Fe – 3.3%. Generally speaking, the porosity of the samples doped with iron is very small. It slightly increases with the increase of the iron content and for the 94YSZ6Fe sample reaches 4.2%. Samples with chromium are showing much higher porosities. The 99YSZ1Cr sample sintered at 1400 °C has the porosity of 6.2%, while the porosity of the 94YSZ6Cr sample has reached 19%. It means that the presence of chromium constraints the sintering process of the pellets. For samples sintered at 1200 °C the lowest porosity is obtained for 94YSZ6Fe, which is 7% in comparison to 35% and 54% for pure and 94YSZ6Cr samples, respectively. From this data it can be deduced that iron effectively

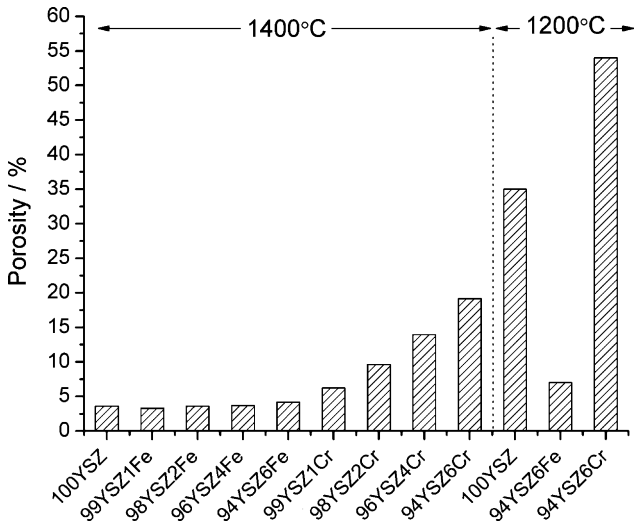

Fig. 2. Porosity of all of the prepared samples sintered at 1200 °C and 1400 °C.

promotes sintering of the electrolyte material while chromium drastically reduces sinterability. These differences might be due to the difference in the melting points of the oxides, i.e. 1566 °C and 2435 °C for iron oxide and chromium oxide, respectively. Iron oxide, with low melting temperature, may act as a promoter of mass transport during high temperature sintering. Samples prepared with the addition of iron can be almost fully densified at temperatures even

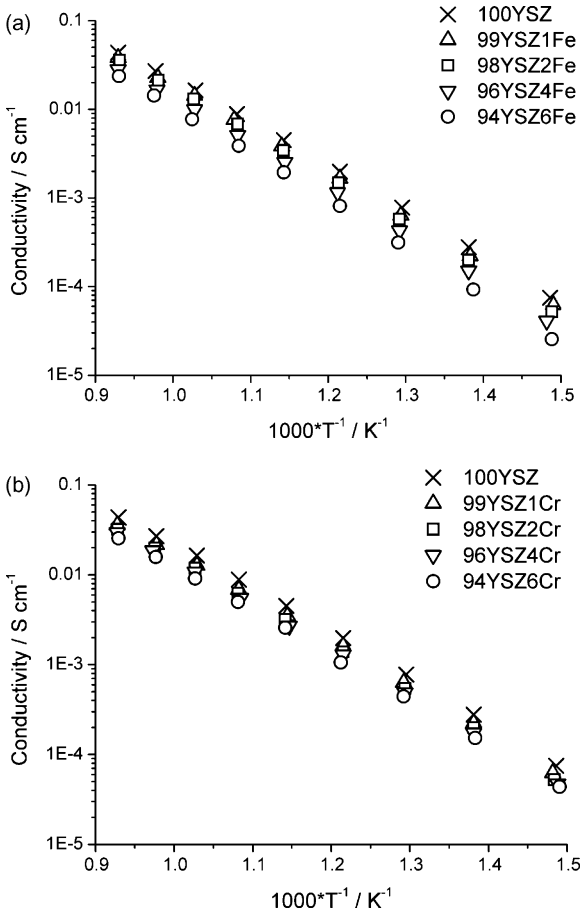

Fig. 3. Total electrical conductivities of samples doped with iron (a) and chromium (b) measured by a van der Pauw technique for samples sintered at 1400 °C.

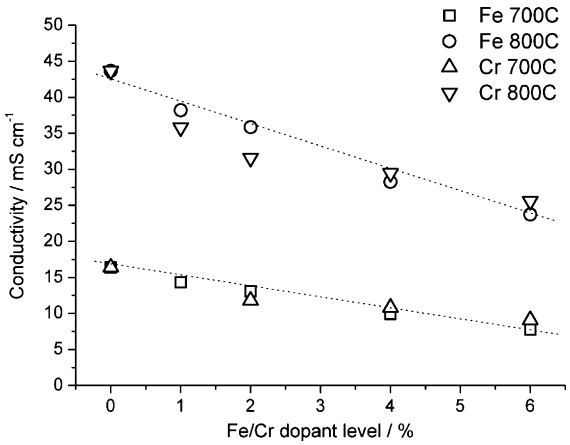

Fig. 4. Total electrical conductivity at 700 °C and 800 °C as a function of iron and chromium content.

200 °C lower than used for normal YSZ powders, which for some applications may be very important.

Total electrical conductivities measured by DC van der Pauw technique for samples sintered at 1400 °C are shown in Fig. 3a and b. In the case of the doped samples, the electrical conductivity was smaller than that of the pure YSZ. The lowest values of the conductivity were observed for the samples containing 6 mol% of iron or chromium. The dependence of the conductivity values at 800 °C and 700 °C on the metal dopant content is given in Fig. 4. It is clearly seen that additives of both dopants change the total conductivity in a similar manner. Based on the data shown in Fig. 3 the activation energy of the total conductivity of the studied samples were determined. The obtained data are plotted in Fig. 5. Activation energies of total conductivities of chromium-doped samples are around 0.99 eV which is very close to that of the pure YSZ. For iron-doped samples activation energies increase from 0.99 eV for 100YSZ up to 1.06 eV for 94YSZ6Fe. It is worth noting that the influence of iron doping on the activation energy of total conductivity is much stronger than that of chromium doping. In contrary to this result, in work by Matsui [13] a decrease of activation energy upon doping by iron was reported. Also very interesting is the comparison of electrical conductivity with respect to measured porosity, which for chromium-doped samples was much higher than for the other samples. It is rather unexpected that the 94YSZ6Cr sample with 19% porosity has comparable conductivity with the 94YSZ6Fe sample with only 4.2% porosity.

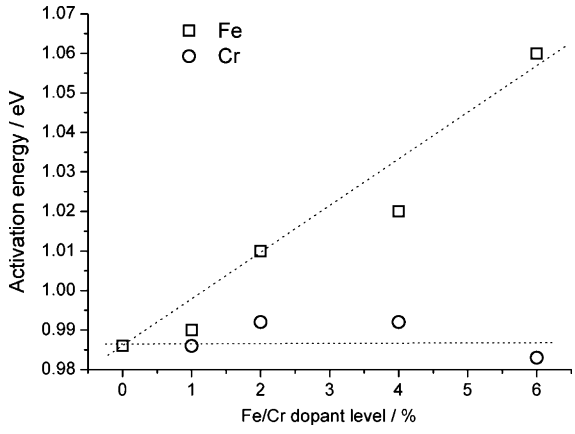

Fig. 5. Activation energy of total electrical conductivity for iron and chromium-doped samples sintered at 1400 °C.

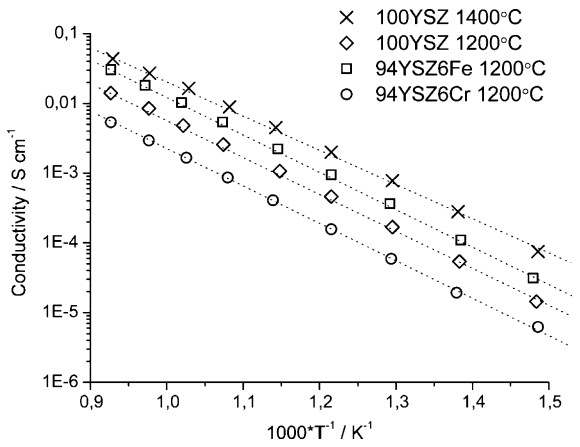

Fig. 6. Temperature dependence of total electrical conductivities of the samples sintered at 1200 °C.

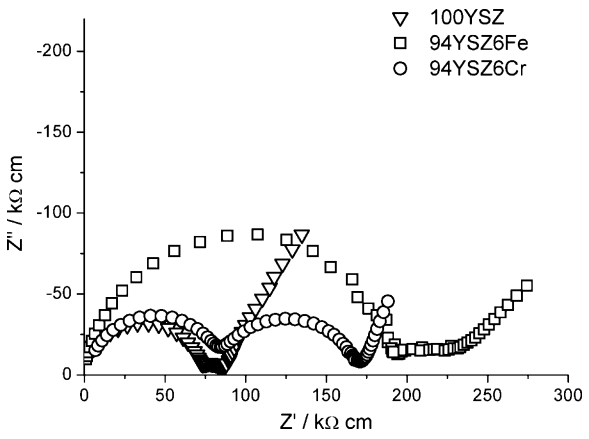

Fig. 7. Typical impedance spectra by Nyquist diagrams of samples sintered at 1400 °C. Measurements were performed at 285 °C.

The total conductivity of the samples sintered at 1200 °C as a function of temperature is presented in Fig. 6. For comparison, also the data of undoped YSZ sintered at 1400 °C are shown. It can be seen that the samples sintered at 1200 °C behave in a different way than those sintered at higher temperature. For example, the 94YSZ6Fe sample sintered at 1200 °C has conductivity higher than pure YSZ sintered at 1200 °C but lower than pure YSZ sintered at 1400 °C. The effect of improved density probably plays in this case an important role, counterbalancing the negative effect of iron on conductivity what is the case for samples sintered at 1400 °C. Chromium-doped sample has the smallest conductivity. What is interesting, activation energies of the conductivity of all the samples are similar (1.07 eV).

To determine the influence of iron and chromium dopants on the grain and grain boundary conductivity impedance spectroscopy experiments were conducted. In this case a difference in grain/grain boundary resistance was expected to be dependent of metal cation content. Typical impedance spectra measured at 285 °C for the 100YSZ, 94YSZ6Fe and 94YSZ6Cr samples are shown in Fig. 7. For all samples two semicircles and low frequency electrode response tail are easily distinguished. High frequency semicircle is attributed to grains while medium frequency semicircle represents grain boundary contribution. For the100YSZ sample grain resistance is

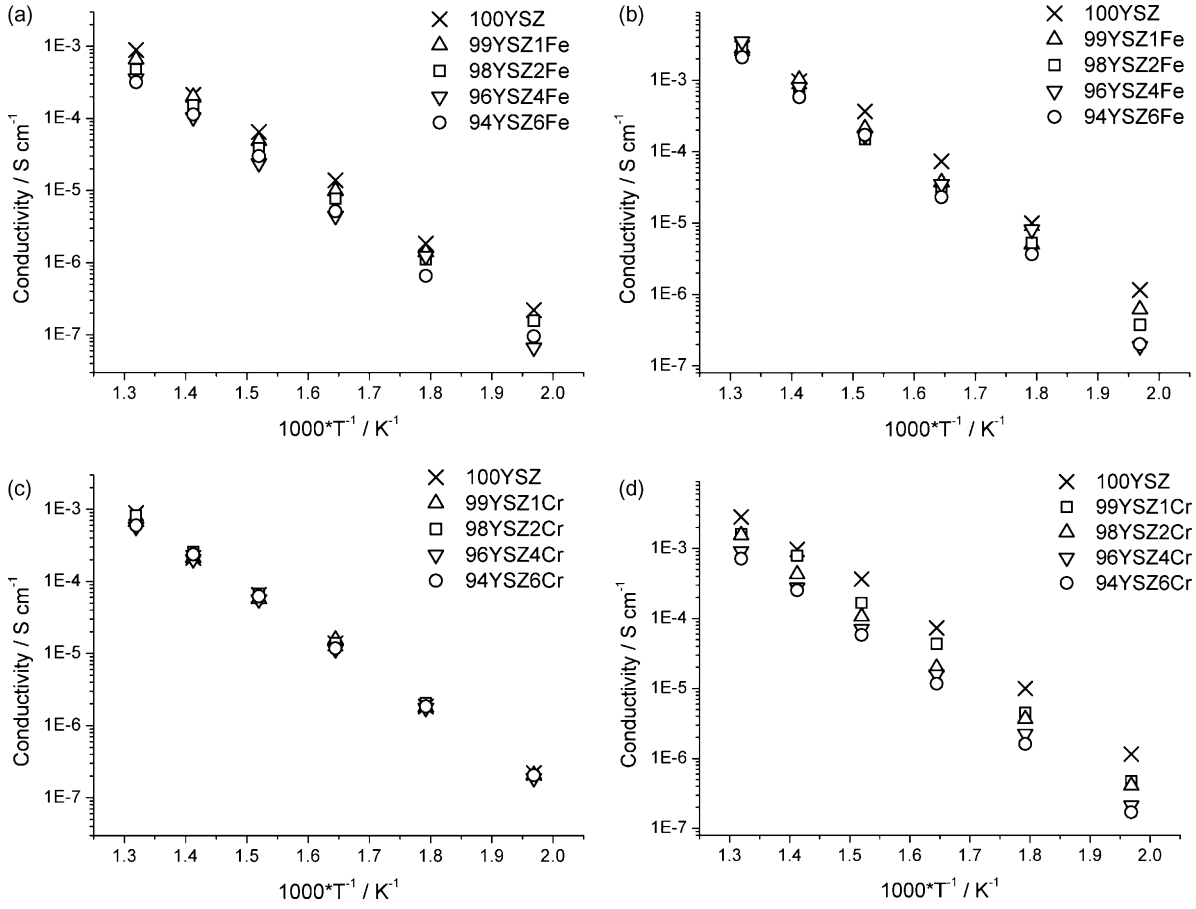

Fig. 8. Grain (a and c) and grain boundary (b and d) electrical conductivities of iron and chromium-doped samples.

much higher than the grain boundary resistance. Sample 94YSZ6Cr shows grain contribution similar to the undoped YSZ sample while grain boundary contribution is comparable to the grain part. From this data it may be concluded that chromium dopant influence mainly grain boundaries. This is supported by the data presented in Fig. 8a–d. In which temperature dependence of the grain and grain boundary conductivities calculated on the basis of the impedance spectra are shown. In the case of chromium-doped samples grain conductivity does not depend on the chromium content (Fig. 8c). This is somewhat contrary to the refined unit cell parameter results. Namely, the chromium-doped samples show lattice contraction, which can be connected to dissolution of Cr into YSZ crystallites. Both the values and the activation energy of electrical conductivity are similar for all the samples. In contrast to the grain conductivity of Cr-doped YSZ, the grain boundary conductivity (Fig. 8d) decreases monotonically with the dopant content. In the case of iron-doped samples, grain contribution (Fig. 8a) changes monotonically with the increase of iron content, while the grain boundary conductivity (Fig. 8b) is affected only up to about 2 mol% of Fe. It indicates that iron is segregated and some allocates in the grain boundary with a solubility limit in this region, while the rest of iron is dissolved in the YSZ grains. These differences in solubility in grain and grain boundaries result in an unknown content of appropriate dopant in YSZ phase. The influence of iron on the grain and grain boundary conductivities differs from the one reported by Matsui [13]. In his case the more iron was added the lower grain boundary resistance was measured. Grains were also affected by iron but no dependency on the amount of iron on the resistance was found. Differences concerning grain boundary conductivity need to be explained by further studies.

4. Conclusions

Addition of Fe_2O_3 and Cr_2O_3 to the YSZ, followed by high temperature sintering cause full dissolution of these metal oxides into grains and/or grain boundaries. This is evidenced by XRD patterns, where only single-phase material is observed. For both dopants a contraction of the lattice parameter is observed for all doping levels, as calculated by Rietveld refinement. However AC electrical measurements show that the mechanism of electrical conduction in iron and chromium-doped samples is different. In the case of iron, it seems that there exists a solubility limit for Fe at grain boundaries, estimated at about 2 mol% with no limit for grains in the studied range. Addition of chromium affects mainly grain boundaries. Both oxide additives lower the total electrical conductivities of samples. Fe addition also changes the activation energy of samples. It was also evaluated that iron is a sintering promoter while chromium restrains sintering of YSZ powders.

Acknowledgement

This project is supported by Ministry of Higher Education under the grant No. N511 376135.

References

[1] S.M. Haile, Acta Mater. 51 (2003) 5981–6000.
[2] M.D. Anderson, J.W. Stevenson, S.P. Simner, J. Power Sources 129 (2004) 188–192.
[3] J.H. Kim, G.M. Choi, Solid State Ionics 130 (2000) 157–168.
[4] K. Kobayashia, S. Yamaguchia, T. Higuchi, S. Shin, Y. Iguchi, Solid State Ionics 135 (2000) 643–651.
[5] J.W. Fergus, Mater. Sci. Eng. A 397 (2005) 271–283.
[6] S. Molin, B. Kusz, M. Gazda, P. Jasinski, J. Power Sources 181 (2008) 31–37.
[7] S. Davison, R. Kershaw, K. Dwight, A. Wold, J. Solid State Chem. 73 (1988) 47–51.
[8] F.J. Berry, M.H. Loretto, M.R. Smith, J. Solid State Chem. 83 (1989) 91–99.
[9] N. Gokon, T. Mizuno, Y. Nakamuro, T. Kodama, J. Sol. Energy Eng. 130 (2008), 011018-1-011018-6.
[10] H. Nakajima, K. Itoh, H. Kaneko, Y. Tamaura, J. Phys. Chem. Solids 68 (2007) 1946–1950.
[11] H. Gao, J. Liu, H. Chen, S. Li, T. He, Y. Ji, J. Zhang, Solid State Ionics 179 (2008) 1620–1624.
[12] N.M. McDonald, J. Liu, G. Gratson, S.A. Barnett, Fuel Cell Seminar, Abstracts, Palm Springs, CA, November 18–21, 2002, p. 510.
[13] N. Matsui, Denki Kagaku 59 (1991) 31.
[14] N. Matsui, Denki Kagaku 60 (1992) 639.
[15] R.V. Wilhelm Jr., D.S. Howarth, Am. Ceram. Soc. Bull. 58 (1979) 228.